

Effective mass of heavy, light, and spin split-off band electron and hole g-factor in cubic perovskite materials

Cite as: J. Appl. Phys. **128**, 235109 (2020); <https://doi.org/10.1063/5.0028266>

Submitted: 07 September 2020 . Accepted: 27 November 2020 . Published Online: 21 December 2020

 David Ompong,  Godfred Inkoom, and  Jai Singh



View Online



Export Citation



CrossMark

ARTICLES YOU MAY BE INTERESTED IN

Theoretical investigations of structural, electronic, and physical properties of Rb_2BX_6 ($\text{B}=\text{Ti}$, Se , Pd ; $\text{X}=\text{F}$, Cl , Br , I) double perovskites

Journal of Applied Physics **128**, 235110 (2020); <https://doi.org/10.1063/5.0024953>

Phonon transport in antisite-substituted hexagonal boron nitride nanosheets: A molecular dynamics study

Journal of Applied Physics **128**, 234304 (2020); <https://doi.org/10.1063/5.0025402>

Monte Carlo simulations of phase transitions and nucleation

Journal of Applied Physics **128**, 235108 (2020); <https://doi.org/10.1063/5.0034744>

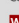

HIDEN
ANALYTICAL

Instruments for Advanced Science

- Knowledge,
- Experience,
- Expertise

Click to view our product catalogue

Contact Hiden Analytical for further details:

 www.HidenAnalytical.com
 info@hiden.co.uk

Gas Analysis

- ▶ dynamic measurement of reaction gas streams
- ▶ catalysis and thermal analysis
- ▶ molecular beam studies
- ▶ dissolved species probes
- ▶ fermentation, environmental and ecological studies

Surface Science

- ▶ UHVTPD
- ▶ SIMS
- ▶ end point detection in ion beam etch
- ▶ elemental imaging - surface mapping

Plasma Diagnostics

- ▶ plasma source characterization
- ▶ etch and deposition process reaction kinetic studies
- ▶ analysis of neutral and radical species

Vacuum Analysis

- ▶ partial pressure measurement and control of process gases
- ▶ reactive sputter process control
- ▶ vacuum diagnostics
- ▶ vacuum coating process monitoring



Effective mass of heavy, light, and spin split-off band electron and hole g-factor in cubic perovskite materials

Cite as: J. Appl. Phys. 128, 235109 (2020); doi: 10.1063/5.0028266

Submitted: 7 September 2020 · Accepted: 27 November 2020 ·

Published Online: 21 December 2020



David Ompong,¹ Godfred Inkoom,² and Jai Singh^{1,a)}

AFFILIATIONS

¹College of Engineering, IT and Environment, Charles Darwin University, Darwin, NT 0909, Australia

²Department of Physics & Astronomy, Mississippi State University, Starkville, Mississippi 39762-5167, USA

^{a)}Author to whom correspondence should be addressed: jai.singh@cdu.edu.au

ABSTRACT

Analytical expressions for the effective mass of heavy, light, and spin split-off electrons are obtained by diagonalizing the $\mathbf{k} \cdot \mathbf{p}$ Hamiltonian for cubic perovskite crystal structures and used to calculate these in nine perovskite materials. An expression for the effective hole g-factor is also derived and calculated in these perovskites. The calculated effective mass of heavy electrons ranges from $1.619 m_0$ to $0.201 m_0$, of light electrons from $0.357 m_0$ to $0.146 m_0$, and of spin split-off electrons from $0.584 m_0$ to $0.169 m_0$. It is found that Cl- and Pb-based perovskite materials have larger heavy, light, and spin split-off electron effective masses. It is also found that the effective g-factor increases with the atomic size, from Cl to I, for the series CsSnX_3 ($X = \text{Cl, Br, I}$).

Published under license by AIP Publishing. <https://doi.org/10.1063/5.0028266>

I. INTRODUCTION

Theoretical and experimental works on semiconductors such as Si, Ge, GaAs, and InSb under stress have provided useful insight and detailed understanding of their band structures.¹ On the theory side, the $\mathbf{k} \cdot \mathbf{p}$ method has been very useful for studying the energy band structures and physical phenomena occurring near the center of the Brillouin zone (BZ) of semiconductors.^{1–3} Recently, perovskite semiconductors have been used in several applications, for example, in solar cells, lasers, photo-rechargeable batteries, and light emitting diodes (LEDs).^{3–7} The $\mathbf{k} \cdot \mathbf{p}$ method has also been used to study the electronic and optical properties of perovskites without including the effect of charge carrier scattering by optical phonons.^{3,8} The finding of large effective masses along some principal axes in perovskite materials has been reported as anomalies.⁸ Density functional theory and quasiparticle self-consistent GW electronic structure calculations have been used to study the electronic transport properties in halide cubic perovskites CsSnX_3 ($X = \text{Cl, Br, I}$),⁹ and it has been found that increasing X results in decreasing the effective masses of heavy and light electrons in the conduction band (CB) along the [100] and [111] directions. As the electron mobility (μ) and the effective mass (m_e) are related by $\mu = \frac{e\tau}{m_e}$, where e is the electronic charge and τ is the

electron scattering time, any change in the effective mass of an electron is expected to influence the mobility, which in turn affects the optoelectronic properties of perovskite devices.^{9–11} As a result, a semiconductor with an anisotropic electron effective mass will have anisotropic mobility leading to anisotropic charge density.^{11–14} Therefore, the effective mass and bandgap energy are among the most important parameters needed to characterize any semiconductor material.

The effective mass of an electron in the CB at a point $\mathbf{k} = \mathbf{k}_0$ is given by $\frac{\hbar^2}{\left(\frac{\partial^2 E(\mathbf{k})}{\partial k^2}\right)\big|_{\mathbf{k}=\mathbf{k}_0}}$, where $\hbar = h/2\pi$ is the reduced Planck's constant and $E(\mathbf{k})$ is the electron energy obtained from the dispersion relation at wavevector \mathbf{k} ; hence, it depends on the electronic band structure.¹⁵ It has been established that the presence of mechanical strain and spin-orbit coupling (SOC) can reduce the crystal symmetry¹ and split the electronic energy bands. However, in perovskites, the splitting of the conduction band due to strain field is found to be relatively small compared to that due to the SOC.³ The magnitude of the strain field is not given here because the influence of hydrostatic, uniaxial, and shear strain on the unstrained crystal potential and their effects on the optoelectronic properties^{2,3} of perovskite heterostructures will be considered in a future study.

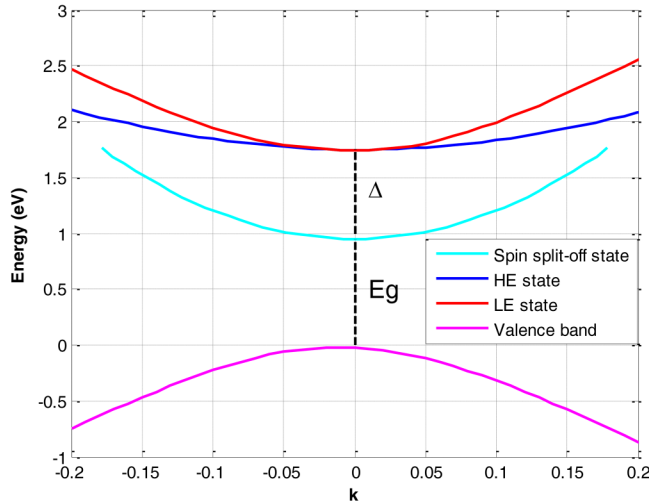


FIG. 1. Schematic band structure of the valence and conduction bands in perovskite materials.

Using band theory calculation including the electron–electron interaction and SOC, it is found that the holes in the valence band of perovskite materials have angular momentum eigenvalue $J = \frac{1}{2}$, whereas the electrons in the conduction band have eigenvalue $J = \frac{3}{2}$. This is similar but opposite to the case of electrons and holes in many III–V semiconductors, where the holes have $J = \frac{3}{2}$ and electron has $J = \frac{1}{2}$.⁴ In perovskite materials, the vectorial representation of the conduction band minimum at the R-point splits into spin-split off (SO), light electron (LE), and heavy electron (HE) electron bands.^{16–18} A schematic band structure of perovskite materials is shown in Fig. 1. However, such a splitting does not occur in the valence band; hence, the valence band is degenerate, isotropic, and parabolic.⁹ To our knowledge, this is the first theoretical study of the effective mass of the heavy, light, and spin split-off electrons and the effective g-factor of holes in perovskite materials. In this paper, we have first derived analytical expressions for the effective mass of heavy, light, and spin split-off electrons and the effective g-factor of holes in cubic perovskite materials for the first time. We have diagonalized the 8×8 matrix Hamiltonian for a cubic perovskite structure with a direct bandgap at the R-point to obtain the analytical expressions, which are then used to calculate the electron effective masses for some inorganic and hybrid organic cubic perovskite materials and effective g-factors of holes. The results of this study may be useful in the design of perovskite-based devices.

II. ELECTRON EFFECTIVE MASS IN CUBIC PEROVSKITE MATERIALS

Luttinger¹⁹ developed the quantum theory of cyclotron resonance using a four-band model for semiconductors with a diamond structure. Pidgeon and Brown²⁰ extended the four-band model to the eight-band model by considering the conduction band together with the degenerate valence band. Accordingly, the band structure of a bulk cubic perovskite semiconductors material

at the R-point can be described by an 8×8 matrix Hamiltonian \hat{H} ^{17,21} given in Table I. The fully coupled Hamiltonian includes double spin-degenerate p -like orbitals of the conduction band HE, LE, and SO bands and s -like orbitals of the valence band.

In Table I,

$$P_{\pm} = P(k_x \pm ik_y), \quad (1)$$

$$P_z = Pk_z + i\delta, \quad (2)$$

$$VB = E_G + \frac{\hbar^2}{2m_0} \gamma_v [k_x^2 + k_y^2 + k_z^2], \quad (3)$$

$$\gamma_v = \frac{1}{m_h} - \frac{E_p}{3} \left(\frac{2}{E_G} + \frac{1}{E_G + \Delta} \right), \quad (4)$$

$$CH = \frac{\hbar^2}{2m_0} [(\gamma_1 + \gamma_2)(k_x^2 + k_y^2) + (\gamma_1 - 2\gamma_2)k_z^2], \quad (5)$$

$$CL = \frac{\hbar^2}{2m_0} [(\gamma_1 - \gamma_2)(k_x^2 + k_y^2) + (\gamma_1 + 2\gamma_2)k_z^2], \quad (6)$$

$$CS = \frac{\hbar^2}{2m_0} [\gamma_1(k_x^2 + k_y^2 + k_z^2)] - \Delta, \quad (7)$$

$$S = \frac{\hbar^2}{2m_0} 2\sqrt{3} \gamma_3 (-k_x + ik_y)k_z, \quad (8)$$

$$R = \frac{\hbar^2}{2m_0} \sqrt{3} [\gamma_2(k_x^2 - k_y^2) - 2i\gamma_3 k_x k_y], \quad (9)$$

$$D = \frac{\hbar^2}{2m_0} \sqrt{2} \gamma_2 (k_x^2 + k_y^2 - 2k_z^2), \quad (10)$$

$$E_p = \frac{2m_0}{\hbar^2} P^2 = \frac{2}{m_0} P_0^2, \quad (11)$$

$$P = -i \frac{\hbar}{m_0} \langle s | p_x | x \rangle, \quad (12)$$

$$p_x = -i\hbar \frac{\partial}{\partial x}. \quad (13)$$

In Table I, $|S \uparrow\rangle$ and $|S \downarrow\rangle$ represent the valence hole states, $|\frac{3}{2} \pm \frac{3}{2}\rangle$ and $|\frac{3}{2} \pm \frac{1}{2}\rangle$ represent the fourfold degenerate heavy and light electron states, and $|\frac{1}{2} \pm \frac{1}{2}\rangle$ and $|\frac{1}{2} - \frac{1}{2}\rangle$ represent spin split-off electrons in the conduction band. The 8×8 matrix Hamiltonian cannot be block diagonalized completely for any arbitrary k ; however, the matrix elements in the Hamiltonian (Table I) can be diagonalized analytically if we consider only small k values,^{2,13} which makes the inter-band matrix elements negligible in comparison with SO coupling. Then, the 8×8 matrix Hamiltonian can be

TABLE I. Matrix Hamiltonian \hat{H} representing the cubic perovskite structure with a direct bandgap at the R-point.¹⁷

	$ S \uparrow\rangle$	$ S \downarrow\rangle$	$ \frac{3}{2} \frac{3}{2}\rangle$	$ \frac{3}{2} \frac{1}{2}\rangle$	$ \frac{3}{2} -\frac{1}{2}\rangle$	$ \frac{3}{2} -\frac{3}{2}\rangle$	$ \frac{1}{2} \frac{1}{2}\rangle$	$ \frac{1}{2} -\frac{1}{2}\rangle$
$\langle S \uparrow $	VB	0	$\frac{1}{\sqrt{2}}P_+$	$-\frac{\sqrt{2}}{\sqrt{3}}P_z$	$-\frac{1}{\sqrt{6}}P_-$	0	$-\frac{1}{\sqrt{3}}P_z$	$-\frac{1}{\sqrt{3}}P_-$
$\langle S \downarrow $	0	VB	0	$\frac{1}{\sqrt{6}}P_+$	$-\frac{\sqrt{2}}{\sqrt{3}}P_z$	$-\frac{1}{\sqrt{2}}P_-$	$-\frac{1}{\sqrt{3}}P_+$	$\frac{1}{\sqrt{3}}P_z$
$\langle \frac{3}{2} \frac{3}{2} $	$\frac{1}{\sqrt{2}}P_-$	0	CH	S	-R	0	$\frac{S}{\sqrt{2}}$	$-\sqrt{2}R$
$\langle \frac{3}{2} \frac{1}{2} $	$-\frac{\sqrt{2}}{\sqrt{3}}P_z$	$-\frac{1}{\sqrt{6}}P_-$	S^*	CL	0	-R	-D	$\frac{\sqrt{3}}{\sqrt{2}}S$
$\langle \frac{3}{2} -\frac{1}{2} $	$-\frac{1}{\sqrt{6}}P_+$	$-\frac{\sqrt{2}}{\sqrt{3}}P_z$	$-R^*$	0	CL	-S	$-\frac{\sqrt{3}}{\sqrt{2}}S^*$	D
$\langle \frac{3}{2} -\frac{3}{2} $	0	$-\frac{1}{\sqrt{2}}P_+$	0	$-R^*$	$-S^*$	CH	$\sqrt{2}R^*$	$\frac{1}{\sqrt{2}}S^*$
$\langle \frac{1}{2} \frac{1}{2} $	$-\frac{1}{\sqrt{3}}P_z$	$-\frac{1}{\sqrt{3}}P_-$	$\frac{1}{\sqrt{2}}S^*$	-D	$-\frac{\sqrt{3}}{\sqrt{2}}S$	$\sqrt{2}R$	CS	0
$\langle \frac{1}{2} -\frac{1}{2} $	$-\frac{1}{\sqrt{3}}P_+$	$\frac{1}{\sqrt{3}}P_z$	$-\sqrt{2}R^*$	$-\frac{\sqrt{3}}{\sqrt{2}}S^*$	D	$\frac{1}{\sqrt{2}}S$	0	CS

partitioned into three intra-band matrices: (1) a 2×2 valence band matrix Hamiltonian (includes first two columns and first two rows of Table I) and (2) a 4×4 matrix Hamiltonian for HE and LE electrons in the conduction band as given in Table II, and (3) a 2×2 matrix Hamiltonian for the spin split-off electrons in the conduction band as given in Table III. Finally, to derive the effective mass of the heavy and light electrons, we diagonalize the 4×4 matrix given in Table II.

By diagonalizing and solving the eigenvalue of the matrix $|H-E(k)| = 0$ in Table II, we get the energy eigenvalue for heavy and light electrons as

$$E(k) = \left(\frac{\hbar^2}{2m_0} \right) \left\{ \gamma_1 k^2 \pm 2 \left(\gamma_2^2 [k_x^2 (k_x^2 - k_y^2) + k_y^2 (k_y^2 - k_z^2)] + k_z^2 (k_z^2 - k_x^2) + 3 \gamma_3^2 (k_x^2 k_y^2 + k_y^2 k_z^2 + k_z^2 k_x^2) \right)^{\frac{1}{2}} \right\}, \quad (14)$$

where $k^2 = k_x^2 + k_y^2 + k_z^2$, m_0 is the free electron mass, and + and - signs in the second term within the bracket are assigned to represent the light and heavy electrons, respectively. In Eq. (14), the normalized Luttinger parameters,¹⁷ γ_i ($i = 1, 2, 3$), are the linearly independent parameters, which determine the curvature of the energy band away from the R-point. Equation (14) is anisotropic unless $\gamma_3 = 0$ and non-parabolic unless both $\gamma_{2,3} = 0$. Equating $E(k)$ on the left hand side of Eq. (14) with the energy of the

electron obtained within the effective mass approximation,

$$E(k) = \frac{\hbar^2 k^2}{2m_{\pm e}}, \quad (15)$$

we get

$$\frac{m_0}{m_{\pm e}} = \left\{ \gamma_1 \pm \frac{2}{k^2} \left(\gamma_2^2 [k_x^2 (k_x^2 - k_y^2) + k_y^2 (k_y^2 - k_z^2)] + k_z^2 (k_z^2 - k_x^2) + 3 \gamma_3^2 (k_x^2 k_y^2 + k_y^2 k_z^2 + k_z^2 k_x^2) \right)^{\frac{1}{2}} \right\}, \quad (16)$$

where $m_{+e} = m_{le}$ and $m_{-e} = m_{he}$ represent the light and heavy electron masses, respectively. From Eq. (16), we can express the effective masses of the heavy and light electrons in the [110] ($k_x = k_y = 1$, $k_z = 0$) direction as

$$m_{he}[110] = \left(\gamma_1 - \sqrt{\gamma_2^2 + 3\gamma_3^2} \right)^{-1} m_0 \quad (17a)$$

and

$$m_{le}[110] = \left(\gamma_1 + \sqrt{\gamma_2^2 + 3\gamma_3^2} \right)^{-1} m_0. \quad (17b)$$

Likewise, to derive the effective mass of the spin split-off electron, we diagonalize the 2×2 matrix in Table III and solve

TABLE II. Matrix Hamiltonian for calculating the effective mass of heavy and light electrons in the conduction band.

	$ \frac{3}{2} \frac{3}{2}\rangle$	$ \frac{3}{2} \frac{1}{2}\rangle$	$ \frac{3}{2} -\frac{1}{2}\rangle$	$ \frac{3}{2} -\frac{3}{2}\rangle$
$ \frac{3}{2} \frac{3}{2}\rangle$	CH	S	-R	0
$ \frac{3}{2} \frac{1}{2}\rangle$	S^*	CL	0	-R
$ \frac{3}{2} -\frac{1}{2}\rangle$	$-R^*$	0	CL	-S
$ \frac{3}{2} -\frac{3}{2}\rangle$	0	$-R^*$	$-S^*$	CH

TABLE III. Matrix Hamiltonian for deriving the effective mass of spin split-off electrons in the conduction band.

	$ \frac{1}{2} \frac{1}{2}\rangle$	$ \frac{1}{2} -\frac{1}{2}\rangle$
$\langle \frac{1}{2} \frac{1}{2} $	CS	0
$\langle \frac{1}{2} -\frac{1}{2} $	0	CS

$|H - E_{SO}(k)| = 0$, which gives

$$E_{SO}(k) = CS = \frac{\hbar^2}{2m_0} [\gamma_1(k_x^2 + k_y^2 + k_z^2)] - \Delta, \quad (18)$$

and then applying the effective mass approximation by writing

$$E_{SO}(k) = \frac{\hbar^2 k^2}{2m_{so}} \quad (19)$$

and equating with Eq. (18), we get the effective mass of the spin split-off electron m_{so} in the conduction band as

$$\frac{m_0}{m_{so}} = \gamma_1 - \frac{2m_0\Delta}{\hbar^2 k^2}, \quad (20)$$

where Δ is the SOC splitting in the CB.

For calculating the effective mass of electrons in the heavy and light from Eq. (16) and spin split-off from Eq. (20) bands, one requires the input parameters that are listed in Table IV for all inorganic and hybrid organic-inorganic perovskite materials known to have a cubic crystal structure. Some of these parameters are extracted from published figures as described below: The bandgap (E_g) and spin-orbit splitting (Δ) energies for the first three materials, CsPbX₃ (X = Cl, Br, I), in Table IV are obtained from Ref. 18 [extracted from Fig. 1(b) in the text and the Extended Data Fig. 1 in the section methods]. For the next three materials, CsSnX₃ (X = Cl, Br, I), and E_g and Δ are obtained from Ref. 9 (E_g is given in Table IV and Δ in Table III of Ref. 9). The effective mass of the valence band hole (m_h) and the Kane energy (E_P) for CsPbX₃ (X = Cl, Br, I) are obtained from the supplementary information (Table S1), and the lattice constants (a) are given under band-structure calculations on the right column of page 194 of Ref. 18. For the next three materials, CsSnX₃ (X = Cl, Br, I), we have calculated E_P from the method described in Sec. I B of the

supplementary information of Ref. 18, and the values of Δ , m_h , and a are given in Tables III, VI, and I, respectively, of Ref. 9.

The Luttinger parameters in Table IV are calculated as follows: Eqs. (7a)–(7d) in Ref. 17 relate the Luttinger parameters with the effective masses in the [100] and [111] directions, which are in turn related to the inverse mass parameters, A, B, and C in Eqs. (2) and (3) of Ref. 9. Therefore, γ_1^L , γ_2^L , and γ_3^L are calculated from the known A, B, and C for all the nine cubic perovskites as

$$\gamma_1^L = \frac{1}{2}(A + B), \quad (21)$$

$$\gamma_2^L = \frac{1}{4}(A - B), \quad (22)$$

$$\gamma_3^L = \frac{1}{4}C. \quad (23)$$

Using Eqs. (21)–(23), the normalized Luttinger parameters γ_1 , γ_2 , γ_3 are obtained as¹⁷

$$\gamma_1 = \gamma_1^L - \frac{1}{3} \frac{E_P}{E_g}, \quad (24)$$

$$\gamma_2 = \gamma_2^L - \frac{1}{6} \frac{E_P}{E_g}, \quad (25)$$

$$\gamma_3 = \gamma_3^L - \frac{1}{6} \frac{E_P}{E_g}. \quad (26)$$

Using Eqs. (24)–(26), the effective masses can be calculated from Eqs. (16) and (20). As explained above, all the parameters in Table IV are calculated theoretically and obtained from references shown in Table IV except the bandgap energies listed in column 3,

TABLE IV. Input parameters for calculating the effective masses of spin split-off, heavy, and light electrons and the effective g-factor of holes in perovskite materials.

	E_g^{theo} (eV)	E_g^{exp} (eV)	Δ (eV)	γ_1^L	γ_2^L	γ_3^L	m_h (m_0)	E_P (eV)	a (Å)
CsPbCl ₃	3.27 ^a	3.04 ^b	1.53 ^a	5.8	2.2	0.5	0.170 ^a	40.1 ^a	5.610 ^a
CsPbBr ₃	2.36 ^a	2.36 ^b	1.50 ^a	7.6	3.0	0.7	0.128 ^a	39.9 ^a	5.865 ^a
CsPbI ₃	2.05 ^a	1.73 ^c	1.44 ^a	9.1	3.6	0.7	0.095 ^a	41.6 ^a	6.238 ^a
CsSnCl ₃	2.69 ^d	...	0.45 ^d	6.4	2.5	0.8	0.140 ^d	34.7	5.560 ^d
CsSnBr ₃	1.38 ^d	...	0.44 ^d	10.2	4.3	1.7	0.082 ^d	35.7	5.804 ^d
CsSnI ₃	1.01 ^d	...	0.42 ^d	13.0	5.6	2.1	0.069 ^d	29.9	6.219 ^d
CH ₃ NH ₃ PbI ₃	1.60 ^e	1.57 ^c	1.40	0.170 ^f	15.3 ^e	6.200 ^e
CsSiI ₃	0.31 ^g	...	0.50	24.3	11.5	8.1	...	18.9	5.892 ^g
CsGeI ₃	1.20 ^g	...	0.27	11.4	5.0	1.4	...	28.2	6.050 ^g

^aReference 18.

^bReference 23.

^cReference 24.

^dReference 9.

^eReference 22.

^fReference 3.

^gReference 5.

which are experimental values. As the experimental E_g is known only for four materials (see Table IV), we have used the theoretical values known for all the materials. However, according to Table IV, the experimental and theoretical values of E_g are in reasonable agreement.

III. HOLE EFFECTIVE g-FACTOR IN CUBIC PEROVSKITE MATERIALS

The effective g-factor for the s-like hole, $g^* = g_0 + g'$, where g' is derived from second-order perturbation theory, is²

$$g' = \frac{g_0}{im_0} \sum_{\alpha} \frac{\langle S \uparrow | p_x | \alpha \rangle \langle \alpha | p_y | S \uparrow \rangle - \langle S \uparrow | p_y | \alpha \rangle \langle \alpha | p_x | S \uparrow \rangle}{E_S - E_{\alpha}}. \quad (27)$$

We assume that the only relevant states to be included in the summation in Eq. (27) are from the heavy, light, and spin split-off states of the conduction band as listed in Table V.

Using Table V in Eq. (27), we obtain

$$g' = \frac{g_0 E_p \Delta}{3E_g(E_g + \Delta)}. \quad (28)$$

It may be noted that according to Eqs. (27) and (28), the effective g-factor $g^* \neq g_0$ only if the spin-orbit interaction Δ is non-zero.

IV. RESULTS AND DISCUSSIONS

We have presented the derivations of the effective masses of heavy-, light- [in Eq. (16)], and spin split-off- [in Eq. (20)] electrons and the effective g-factor of holes in perovskite materials. The calculated effective masses from Eqs. (16) and (20) and the effective g-factor g^* from Eq. (27) are listed in Table VI along with the magnitude of the experimental g-factor of holes in two perovskite materials. The Luttinger parameters γ_i^L ($i = 1, 2, 3$) required to calculate the effective masses from Eqs. (16) and (20) were calculated using the inverse mass parameters A , B , and C of the Kohn–Luttinger Hamiltonian^{9,17} and are listed in Table IV. The A , B , and C of CsSnX_3 ($X = \text{Cl}, \text{Br}, \text{I}$) are listed in Table VII in Ref. 9. It may be noted that the Luttinger–Kohn parameters for the

TABLE V. Matrix elements of the heavy (he), light (le), and spin split-off (so) states for computing g' in cubic crystal perovskite materials from Eq. (27).

	$\langle iS \uparrow p_x \alpha \rangle$	$\langle \alpha p_x iS \uparrow \rangle$	$\langle iS \uparrow p_y \alpha \rangle$	$\langle \alpha p_y iS \uparrow \rangle$
he \uparrow	$\frac{1}{\sqrt{2}} P_0$	$\frac{1}{\sqrt{2}} P_0$	$i \frac{1}{\sqrt{2}} P_0$	$i \frac{1}{\sqrt{2}} P_0$
he \downarrow	0	0	0	0
le \uparrow	0	0	0	0
le \downarrow	$-\frac{1}{\sqrt{6}} P_0$	$-\frac{1}{\sqrt{6}} P_0$	$i \frac{1}{\sqrt{6}} P_0$	$i \frac{1}{\sqrt{6}} P_0$
se \uparrow	0	0	0	0
se \downarrow	$-\frac{1}{\sqrt{3}} P_0$	$-\frac{1}{\sqrt{3}} P_0$	$i \frac{1}{\sqrt{3}} P_0$	$i \frac{1}{\sqrt{3}} P_0$

TABLE VI. Effective masses of heavy electron (m_{he}), light electron (m_{le}), split-off electron (m_{so}), and effective g-factors of holes, calculated using Eqs. (14) and (16), and $g^* = g_0 + g'$. The input values for the calculation are given in Table IV.

	m_{he} (m_0)	m_{le} (m_0)	m_{so} (m_0)	g^* theo (g_0)	g^* exp (g_0)
CsPbCl ₃	1.619	0.357	0.584	1.23	...
CsPbBr ₃	1.605	0.303	0.509	1.60	0.75 ²⁵
CsPbI ₃	1.367	0.254	0.428	1.90	...
CsSnCl ₃	0.687	0.298	0.415	0.77	...
CsSnBr ₃	0.682	0.247	0.362	1.30	...
CsSnI ₃	0.672	0.210	0.319	1.75	...
CH ₃ NH ₃ PbI ₃	0.201	0.146	0.169	1.24	0.41 ²⁶
CsSiI ₃	0.378	0.189	0.251	6.77	...
CsGeI ₃	0.486	0.197	0.280	1.22	...

perovskite $\text{CH}_3\text{NH}_3\text{PbI}_3$ are not known; hence, γ_i^L ($i = 1, 2, 3$) for this perovskite could not be calculated. As CsPbI₃ and $\text{CH}_3\text{NH}_3\text{PbI}_3$ have only Cs and CH_3NH_3 different in their structures, we have assumed that the Luttinger parameters for $\text{CH}_3\text{NH}_3\text{PbI}_3$ are the same as for CsPbI₃ in our calculations.

It may be desirable to point out that although perovskite materials may exist in three phases; orthorhombic (γ -phase), tetragonal (β -phase), and cubic (α -phase), many of them hold their stable structure in the γ -phase.⁵ We have not considered β - and γ -phases here, as the high temperature cubic structure of perovskite materials may be regarded to be an ideal structure to understand the basic properties of perovskites.³ The cubic perovskite materials have smaller effective masses compared with the orthorhombic and tetragonal structures;⁸ therefore, we expect the effective masses of the β - and γ -structures to be larger than the values in Table VI.

It is evident from Table VI that as the atomic size of the halide atom X increases from Cl to I, the effective mass of the heavy, light, and spin split-off electrons decreases. The perovskite with Pb (Ge) of a larger atomic size has a heavier effective mass than that with Sn (Si) of a smaller atomic size. Our results agree with previously simulated effective masses in perovskite materials.⁸ It may also be noted that the Luttinger parameters of Cl-based perovskite materials shown in Table IV are consistently smaller than their Br- and I-based counterparts and that of Pb-based perovskite materials are also consistently smaller than their Sn-based counterparts. This establishes a clear inverse relation between the effective mass and the Luttinger parameters of metal halide perovskites.

In Table VI, we see that g' in Eq. (28) depends on bandgap energy E_g , spin-orbit splitting energy Δ , and the Kane energy E_p . Although the expression of g' in Eq. (28) is the same as the one found for the zinc-blende semiconductors,^{2,13} g' is positive in perovskite materials and negative in zinc-blende semiconductors. The calculated values of the g-factor could be compared with their known experimental values only for CsPbBr₃ and $\text{CH}_3\text{NH}_3\text{PbI}_3$, and the calculated values are about twice the experimental results. We observe that an increase in the atomic size from Cl to I for the series CsSnX_3 ($X = \text{Cl}, \text{Br}, \text{I}$) results in an increase in the effective g-factor. We have also found (see Table VI) that the effective

g-factor of CsSiI_3 is the largest, which is due to the small bandgap E_g in the denominator of Eq. (28).

V. CONCLUSIONS

We have derived expressions for the effective mass of heavy, light, spin split-off electrons and the effective g-factor of holes in cubic perovskite materials. Cl- and Pb-based halide perovskite materials have the largest heavy, light, and split-off electron effective masses. The results of our work may be expected to be useful in simulating the performance of perovskite-based opto-electronic devices.

ACKNOWLEDGMENTS

The authors would like to thank Professor Walter R. L. Lambrecht and Dr. Ling-yi Huang for providing the data used to evaluate the Luttinger parameters of CsBX_3 ($B = \text{Pb, Si, Ge}$, $X = \text{Cl, Br, I}$) and the Kane energy of CsBX_3 ($B = \text{Sn, Si, Ge}$, $X = \text{Cl, Br, I}$).

DATA AVAILABILITY

The data that support the findings of this study are available within the article.

REFERENCES

- ¹T. B. Bahder, *Phys. Rev. B* **41**, 11992 (1990).
- ²L. C. Lew Yan Voon and M. Willatzen, *The k p Method Electronic Properties of Semiconductors* (Springer, Berlin, 2009).
- ³J. Even, L. Pedesseau, J.-M. Jancu, and C. Katan, *Phys. Status Solidi RRL* **8**, 31 (2014).
- ⁴C. Zhang, D. Sun, C. X. Sheng, Y. X. Zhai, K. Mielczarek, A. Zakhidov, and Z. V. Vardeny, *Nat. Phys.* **11**, 427 (2015).
- ⁵L.-y. Huang and W. R. L. Lambrecht, *Phys. Rev. B* **93**, 195211 (2016).
- ⁶H. Mehdizadeh-Rad and J. Singh, *J. Appl. Phys.* **126**, 153102 (2019).
- ⁷S. Ahmad, C. George, D. J. Beesley, J. J. Baumberg, and M. De Volder, *Nano Lett.* **18**(3), 1856 (2018).
- ⁸N. Ashari-Astani, S. Meloni, A. H. Salavati, G. Palermo, M. Grätzel, and U. Rothlisberger, *J. Phys. Chem. C* **121**, 23886 (2017).
- ⁹L.-y. Huang and W. R. L. Lambrecht, *Phys. Rev. B* **88**, 165203 (2013).
- ¹⁰D. Omping and J. Singh, *Org. Electron.* **63**, 104–108 (2018).
- ¹¹H. Mehdizadeh-Rad and J. Singh, *J. Mater. Sci. Mater. Electron.* **30**, 10064 (2019).
- ¹²L. D. Whalley, J. M. Frost, Y.-K. Jung, and A. Walsh, *J. Chem. Phys.* **146**, 220901 (2017).
- ¹³P. Y. Yu and M. Cardona, *Fundamentals of Semiconductors: Physics and Materials Properties*, 4th ed. (Springer, Berlin, 2010).
- ¹⁴P. Azarhoosh, S. McKechnie, J. M. Frost, A. Walsh, and M. v. Schilfgaarde, *APL Mater.* **4**, 091501 (2016).
- ¹⁵J. Singh and K. Shimakawa, *Advances in Amorphous Semiconductors* (Taylor & Francis, London, 2003).
- ¹⁶J. Even, *J. Phys. Chem. Lett.* **6**, 2238 (2015).
- ¹⁷W. J. Fan, *AIP Adv.* **8**, 095206 (2018).
- ¹⁸M. A. Becker, R. Vaxenburg, G. Nedelcu, P. C. Sercel, A. Shabaev, M. J. Mehl, J. G. Michopoulos, S. G. Lambrakos, N. Bernstein, J. L. Lyons, T. Stöferle, R. F. Mahr, M. V. Kovalenko, D. J. Norris, G. Rainò, and A. L. Efros, *Nature* **553**, 189 (2018).
- ¹⁹J. M. Luttinger, *Phys. Rev.* **102**, 1030 (1956).
- ²⁰C. R. Pidgeon and R. N. Brown, *Phys. Rev.* **146**, 575 (1966).
- ²¹Z. G. Yu, *Sci. Rep.* **6**, 28576 (2016).
- ²²R. Ben Aich, S. Ben Radhia, K. Boujdaria, M. Chamarro, and C. Testelin, *J. Phys. Chem. Lett.* **11**, 808 (2020).
- ²³I. P. Pashuk, N. S. Pidzyrajlo, and M. G. Matsko, *Fiz. Tverd. Tela* **23**, 2162 (1981).
- ²⁴G. E. Eperon, S. D. Stranks, C. Menelaou, M. B. Johnston, L. M. Herz, and H. J. Snaith, *Energy Environ. Sci.* **7**, 982 (2014).
- ²⁵V. V. Belykh, D. R. Yakovlev, M. M. Glazov, P. S. Grigoryev, M. Hussain, J. Rautert, D. N. Dirin, M. V. Kovalenko, and M. Bayer, *Nat. Commun.* **10**, 673 (2019).
- ²⁶C. Zhang, D. Sun, Z.-G. Yu, C.-X. Sheng, S. McGill, D. Semenov, and Z. V. Vardeny, *Phys. Rev. B* **97**, 134412 (2018).